5-3

Wigner Monte Carlo Approach to Quantum and Dissipative Transport in Si-MOSFETs

Shunsuke Koba, Hideaki Tsuchiya and Matsuto Ogawa
Department of Electrical and Electronic Engineering, Graduate School of Engineering, Kobe University
1-1, Rokko-dai, Nada-ku, Kobe, 657-8501, Japan
E-mail: 108t224t@stu.kobe-u.ac.jp

***Abstract*—We investigate the influences of quantum transport and scattering effects in Si double-gate MOSFETs based on Wigner Monte Carlo (WMC) approach. It is shown that quantum reflection effect makes significant differences in microscopic features of electron transport between classical and quantum approaches and can even reduce drain current at on-state, but it does not necessarily produce drastic change in macroscopic properties including the drain current. On the other hand, source-drain direct tunneling crucially degrades the subthreshold properties in scaled MOSFETs with sub-10 nm gate length. Furthermore, the ability of the WMC method to describe quantum-classical transition of carrier transport is demonstrated.**

***Index-terms*—Quantum reflection, tunneling, quantum-classical transition, Wigner Monte-Carlo approach**

I. INTRODUCTION

For more than forty years, downscaling of the MOSFETs based on Dennard's scaling law has been the most effective way to improve integrated circuit device performance. However, as the gate length of the MOSFETs has reduced down to 10 nm scale, not only well-known quantum confinement effect and ballistic transport, but also quantum transport effects along the channel direction such as source-drain (SD) direct tunneling, quantum reflection inside the channel and quantum repulsion in the source and drain regions have become more and more important [1-3]. Therefore, to analyze the device performances of future MOSFETs precisely, a device simulation considering scattering and quantum transport effects is indispensable. In this paper, we have developed a quantum transport simulator based on a Wigner Monte-Carlo (WMC) approach, which can fully incorporate quantum transport effects. By using the simulator, we have investigated the influences of quantum transport and scattering effects on electrical characteristics of ultra-short channel Si-MOSFETs. We have also demonstrated that quantum-classical transition of carrier transport in a diffusive transport regime is well described using the WMC method.

II. COMPUTATIONAL METHOD AND MODELS

The WMC method stochastically solves the Wigner transport equation described below.

$$\frac{\partial f_w}{\partial t}+\frac{\hbar k}{m_x^*}\frac{\partial f_w}{\partial x}=Qf_w+Cf_w \tag{1}$$

$$Qf_w=-\frac{1}{\hbar}\int_{-\infty}^{\infty}\frac{dk'}{2\pi}V(x,k-k')f_w(x,k',t) \tag{2}$$

where Qf_w is quantum evolution term, which represents quantum transport effects such as tunneling and reflection. Note that the classical drift term is also included in Qf_w. $V(x,k)$ in Eq. (2) is called non-local potential term and is given by

$$V(x,k)=\int_{-\infty}^{\infty}du\sin(ku)\left[E_n\left(x+\frac{u}{2}\right)-E_n\left(x-\frac{u}{2}\right)\right] \tag{3}$$

where E_n represents potential energy distribution, e.g. the subband energy profile along the channel in MOSFETs. Cf_w in Eq. (1) stands for scattering term. In this study, we used the same scattering probabilities as in the semi-classical MC approach, to make a clear comparison between classical and quantum transport properties in MOSFETs.

Unlike a classical distribution function, Wigner function f_w can have negative values. In order to describe this property, a new particle variable $A_i(t)$, called affinity, is introduced, where i is indices of particles. The affinity physically represents a weight of each particle, and is updated according to the quantum evolution term Qf_w. Accordingly, equations-of-motion for particles during free flight are given as follows [1].

$$\frac{dx_i}{dt}=\frac{\hbar k_i}{m_x^*} \tag{4}$$

$$\frac{dk_i}{dt}=0 \tag{5}$$

$$\sum_{i\in M(x,k)}\frac{dA_i}{dt}=Qf_w(x,k,t) \tag{6}$$

Note that wave number k_i is constant with time as shown in Eq. (5) because the classical drift term is already incorporated in the affinity change via the quantum evolution term of Eq. (6). In other words, quantum transport of carriers is described by the temporal change in the weight of particles moving at a constant velocity.

Fig. 1 shows (a) the device structure and (b) the conduction band structure of silicon used in the simulation. The double-gate structure is employed and gate length is set as 10 nm or 6 nm. In this study, we adopted a mode-space expansion method

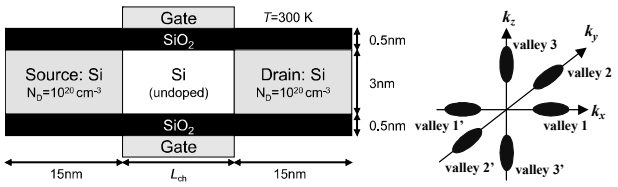

(a) (b)

Fig. 1. (a) Device structure and (b) conduction band structure of silicon used in the simulation. The ellipsoidal multi-valleys and its band nonparabolicity are taken into account. Transport direction is <110>.

This work was supported by the Semiconductor Technology Academic Research Center (STARC).

978-1-61284-418-3/11/$26.00 © 2011 IEEE

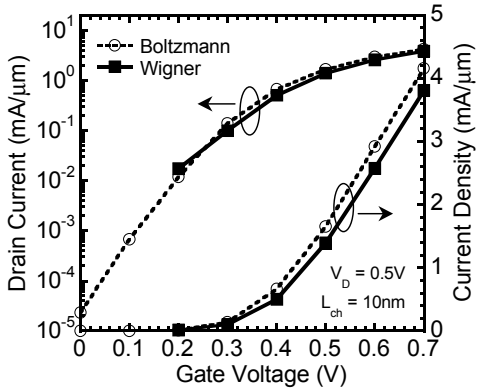

Fig. 2. $I_D - V_G$ characteristics computed for DG-MOSFET with $L_{ch} = 10$ nm. The solid and the dashed lines represent the WMC and the classical MC results, respectively. $V_D = 0.5$ V.

(MSEM) as follows. The device is meshed into vertical slices in which the 1D Schrödinger equation is solved to compute subband profiles and wave-functions. Then, carrier transport is simulated based on the Wigner or Boltzmann MC approach along the channel direction x for each equivalent valley and each subband, where the subband profiles are used as potential energy in Eq. (3). These two MC methods are self-consistently coupled with the 2D Poisson's equation. As for scattering processes, we considered acoustic phonons, non-polar optical phonons, and impurity scatterings. Due to the strong quantization effect in the ultra-thin body channel as T_{ch} = 3nm, most electrons are distributed in the lowest subbands of each valley, and therefore we considered the lowest and first-higher subbands in each valley in the present simulation.

III. Results and Discussion

A. Quantum Transport Effects in 10 nm Channel MOSFET

Fig. 2 shows the $I_D - V_G$ characteristics computed for 10 nm channel DG-MOSFET. V_D is set at 0.5 V throughout this paper. First, it is found that drain current at high gate voltage is reduced in the quantum approach by about 8 % for the present device with L_{ch} = 10 nm, which is mainly due to quantum reflection in the channel as will be discussed later. On the other hand, the subthreshold current is likely to slightly increase in the quantum approach, since the SD direct tunneling is included. Fig. 3 shows (a) the lowest subband energy, (b) sheet carrier density and (c) averaged electron velocity profiles computed at V_G = 0.5 V. As shown in Fig. 3 (b), electron density in the channel exhibits no significant difference between the quantum and classical approaches because of the on-state. However, carrier depletion region in the source and drain is

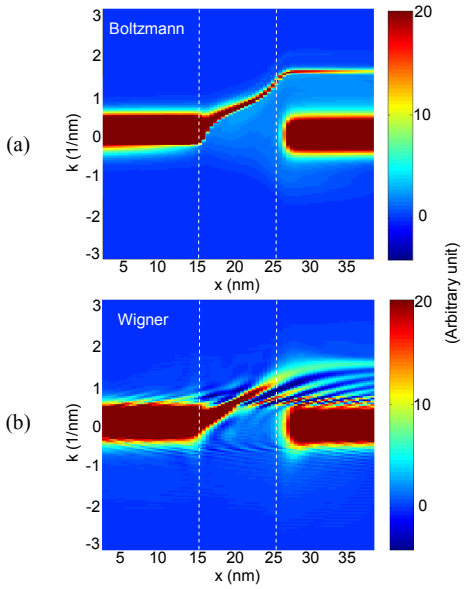

Fig. 4. (a) Classical distribution function and (b) Wigner distribution function in phase space. L_{ch} = 10 nm and $V_G = V_D$ = 0.5 V. Note that all of subbands and valleys are summed up, but most electrons are distributed in the lowest subband.

expanded due to non-local quantum repulsive force from the channel potential [3] as seen in the inset of Fig. 3 (b). Here, note that the averaged electron velocity decreases around the source-end bottleneck barrier by including quantum transport effects as shown in Fig. 3 (c). This is considered due to quantum reflection caused by the steep potential drop inside the channel as shown in Fig. 3 (a). To confirm that the quantum reflection actually happens, we plot distribution functions in phase-space computed by using the classical MC and the WMC methods in Figs. 4 (a) and (b), respectively, where contrast represents the number of electrons present in a cell of the phase space. We can observe distinct oscillations in the Wigner distribution function, while they are not present in the Boltzmann distribution function. In particular, oscillations are visible not only in $k > 0$ region but also in $k < 0$ region, which is the signature of quantum reflection [1]. They occur in the region where the potential abruptly drops between the barrier top and the drain-end of the channel. Accordingly, the quantum reflection indeed decreases the source-end electron velocity and the drain current at on-state compared to the classical one, as shown in Fig. 2.

B. Quantum-Classical Transition under Diffusive Transport

Here, we examine how the carrier scattering influences

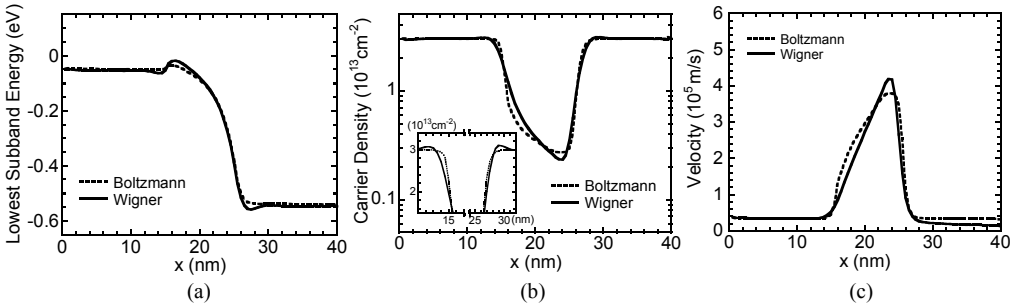

Fig. 3. (a) Lowest subband energy, (b) sheet carrier density and (c) averaged electron velocity profiles for L_{ch} = 10 nm. V_G = 0.5 V and V_D = 0.5 V.

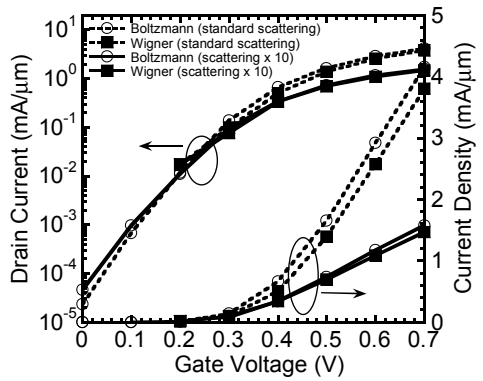

Fig. 5. $I_D - V_G$ characteristics computed by using the increased scattering rate (scattering × 10). For comparison, the previous results using the standard scattering rate are also plotted. L_{ch} = 10 nm.

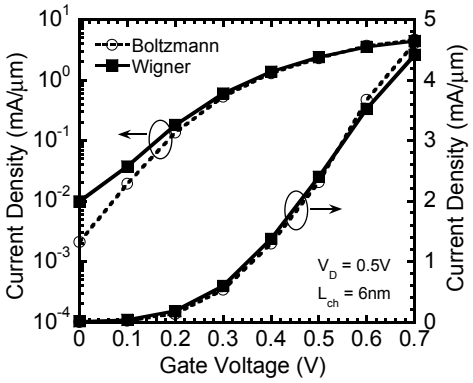

Fig. 7. $I_D - V_G$ characteristics for L_{ch} = 6 nm. The solid and the dashed lines represent the WMC and the classical MC results, respectively.

quantum reflection. To this end, we increased the scattering rate by ten times, which emulates a diffusive transport such as in longer channel devices or higher-temperature operations etc. Fig. 5 shows the $I_D - V_G$ characteristics computed using increased scattering rate (scattering × 10), where the previous results with standard scattering rate are also plotted for comparison. It is found that current reduction at high gate voltage becomes less significant by increasing the scattering rate, and hence the quantum $I_D - V_G$ curve approaches the classical one. This means that quantum reflection vanishes and carrier transport is varied from quantum to classical behaviors under the diffusive transport. Such quantum-classical transition is more clearly observed in the distribution functions as shown in Fig. 6. We can see that quantum interference pattern in the Wigner distribution function completely disappears and classical distribution function is reproduced. As presented above, the WMC method can describe quantum-classical transition of carrier transport.

Furthermore, by limiting our discussion to the classical simulation, the subthreshold slope (SS) is hardly changed with scattering rate as shown in Fig. 5. This is because the subthreshold current is governed by thermally diffusive injection of carriers from the source in the classical limit [4].

C. *Quantum Transport Effects in 6 nm Channel MOSFET*

We further simulated an ultimately scaled device with L_{ch} = 6 nm. Fig. 7 shows the $I_D - V_G$ characteristics, where the subthreshold property is successfully calculated until V_G = 0 V with the WMC method. First, the SS value obviously increases in the quantum approach, since SD direct tunneling is included. On the other hand, the quantum current at high gate voltage has more or less the same value as the classical one. To understand this behavior, the distribution functions at V_G = 0.5 V are calculated as shown in Fig. 8. It is found that quantum interference pattern caused by the quantum reflection is less observable in Fig. 8 (b). This implies that quantum reflection is suppressed in such ultimately scaled device as L_{ch} = 6 nm. Then, we actually calculated the corresponding transmission probabilities for L_{ch} = 6 nm and 10 nm by using a transfer-matrix method as shown in Fig. 9, where the lowest subband profile resulting from the WMC simulation is substituted into Schrödinger equation. In Fig. 9, the energy reference (E = 0) corresponds to the bottom of the bottleneck barrier as indicated

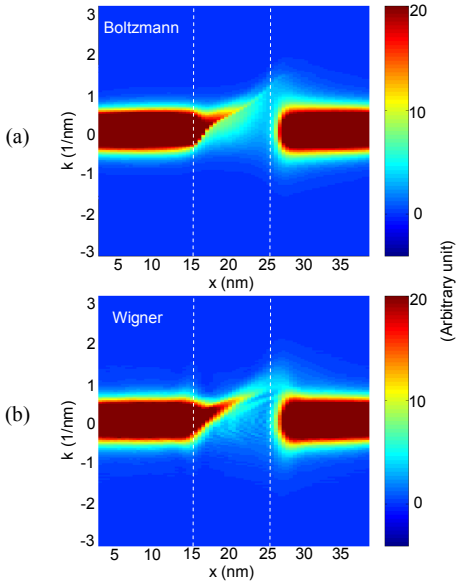

Fig. 6. (a) Classical distribution function and (b) Wigner distribution function in phase space computed using the scattering rate increased by ten times.

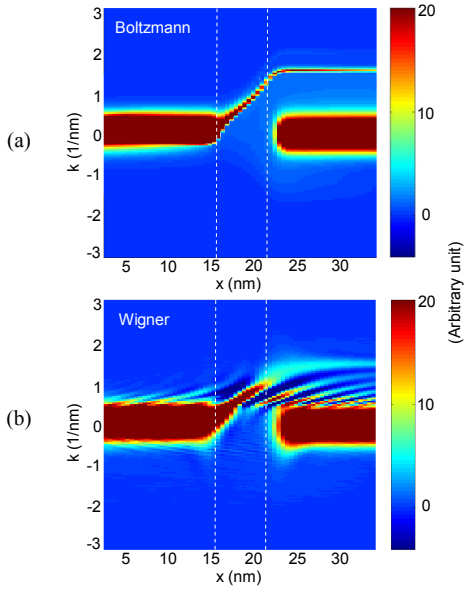

Fig. 8. (a) Classical distribution function and (b) Wigner distribution function in phase space. L_{ch} = 6 nm and $V_G = V_D$ = 0.5 V.

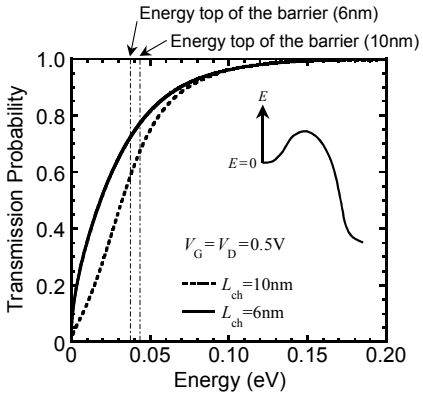

Fig. 9. Transmission probabilities computed using transfer-matrix method at on-state. The solid and the dashed lines correspond to L_{ch} = 6 nm and 10 nm devices, respectively.

in the inset. It is found that even if the kinetic energy becomes larger than energy top of the bottleneck barrier, the transmission probabilities exhibit less than one, and several 10 % of electrons are reflected toward the source for both channel lengths. This is termed quantum reflection. Here, it should be noted that the transmission probability above the energy top of the barrier increases with decreasing the channel length, which indicates that the quantum reflection is receded in the 6 nm device as expected above. Consequently, the reduction in the drain current due to quantum reflection is less pronounced in the present 6 nm device.

Finally, we present the transport properties at off-state. Fig. 10 shows (a) the lowest subband energy, (b) sheet carrier density and (c) averaged electron velocity profiles computed at V_G = 0.1 V, and Fig. 11 the corresponding distribution functions. From Fig. 10 (b), the electron density in the channel obviously increases due to the SD tunneling effect, and as a result the averaged electron velocity significantly decreases because tunneling electrons are not accelerated during the tunneling process. Such tunneling electron trajectory appears in the Wigner distribution function as shown in Fig. 11 (b). Although weak interference pattern is visible in the channel region, an electron trajectory flowing into the drain with acceleration is not observed.

The above results indicate that the SD tunneling becomes more important, while the quantum reflection has less impact on the electrical characteristics, when the channel length is scaled less than 10 nm.

IV. Conclusion

By using the WMC quantum simulator, we have demonstrated that the quantum reflection makes significant differences in the microscopic features of electron transport and can even reduce the drain current at on-state, but it does not necessarily produce drastic change in the macroscopic properties including the drain current. On the other hand, the SD tunneling plays a crucial role in the subthreshold properties of scaled MOSFETs with sub-10 nm gate length. We have also shown that the WMC approach has the ability to describe quantum-classical transition of carrier transport in the diffusive transport regime dominated by scattering.

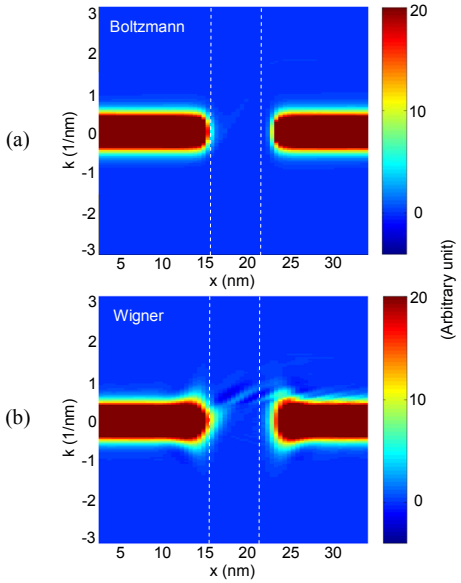

Fig. 11. (a) Classical distribution function and (b) Wigner distribution function in phase space. L_{ch} = 6 nm, V_G = 0.1 V and V_D = 0.5 V.

Acknowledgment

This work was supported by the Semiconductor Technology Academic Research Center (STARC).

References

[1] D. Querlioz and P. Dollfus, *The Wigner Monte Carlo Method for Nanoelectronic Devices* (Wiley, New York, 2010.)

[2] H.-N. Nguyen, D. Querlioz, S. G.-Retailleau, and P. Dollfus, *IEEE Trans. Electron Devices* **58** (2011) 798.

[3] S. Koba, R. Aoyagi, and H. Tsuchiya, *J. Appl. Phys.* **108** (2010) 064504.

[4] Y. Yamada, H. Tsuchiya, and M. Ogawa, *IEEE Trans. Electron Devices* **56** (2009) 1396.

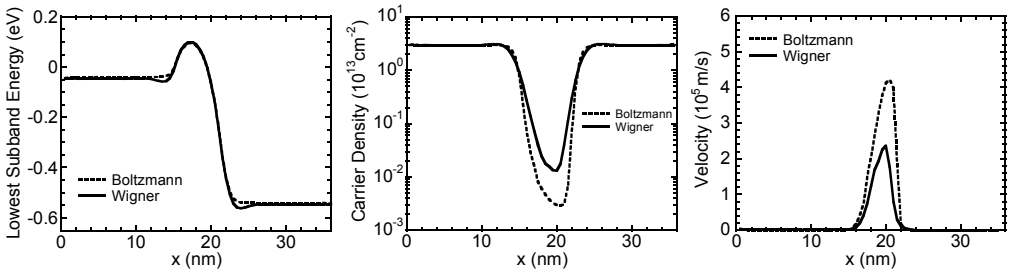

Fig. 10. (a) Lowest subband energy, (b) sheet carrier density and (c) averaged electron velocity profiles for L_{ch} = 6 nm. V_G = 0.1 V and V_D = 0.5 V.